Structure and Properties of α- and β-CeCuSn: A Single Crystal and Mössbauer Spectroscopic Investigation

C. Peter Sebastian, Sudhindra Rayaprol, Rolf-Dieter Hoffmann, Ute Ch. Rodewald, Tania Pape, and Rainer Pöttgen

Institut für Anorganische und Analytische Chemie and NRW Graduate School of Chemistry, Universität Münster, Corrensstraße 30, D-48149 Münster, Germany

Reprint requests to R. Pöttgen. E-mail: pottgen@uni-muenster.de

Z. Naturforsch. **2007**, *62b,* 647 – 657; received December 15, 2006

Two modifications of CeCuSn were prepared from the elements: the high-temperature (β) modification crystallizes directly from the quenched sample, while the low-temperature (α) modification is formed after annealing at 700 °C for one month. Both modifications were investigated by powder and single crystal X-ray diffraction. We find for β-CeCuSn the ZrBeSi-type structure, space group $P6_3/mmc$, a = 458.2(1), c = 793.7(2) pm, w$R2$ = 0.0727, 148 F^2 values, 8 variable parameters. In the case of α-CeCuSn we find the NdPtSb-type structure, space group $P6_3mc$, a = 458.4(1), c = 785.8(2) pm, w$R2$ = 0.0764, 233 F^2 values, 11 variable parameters. The copper and tin atoms build up layers of ordered $[Cu_3Sn_3]$ hexagons. The layers are planar in β-CeCuSn, however, with highly anisotropic displacements of the copper and tin atoms. In α-CeCuSn a puckering effect is observed resulting in a decrease of the c lattice parameter. Both modifications of CeCuSn exhibit antiferromagnetic ordering, but there is a considerable difference in their magnetic behaviour. Anomalies in the physical properties of the α- and β-modifications of CeCuSn have been detected by Mössbauer spectroscopy and magnetic and specific heat measurements, which serve to explain the structure-property relations.

Key words: Stannides, Crystal Structure, Magnetism

Introduction

The *R*CuSn stannides (*R* = rare earth element) have been studied extensively in recent years with respect to their interesting magnetic and electrical properties. An overview of the literature is given in [1]. If the rare earth elements are trivalent, the *R*CuSn stannides crystallize with superstructures [2] that derive from the well known AlB_2-type. The hexagonal structures have AB-AB stacking sequences of planar (ZrBeSi-type [3]) or puckered (NdPtSb- [4] or LiGaGe- [5, 6] type, depending on the degree of puckering) $[Cu_3Sn_3]$ hexagons, which are rotated by 60° in every other layer. The degree of puckering strongly depends on the size of the rare earth element. With lanthanum almost planar layers have been observed [1, 7], while ScCuSn shows a strong puckering, leading to a slightly elongated tetrahedral [CuSn] network [1].

CeCuSn has most thoroughly been investigated [8 – 21], but the structure of CeCuSn has so far only been studied on the basis of powder diffraction data, *i. e.* laboratory X-ray, synchrotron, and neutron powder diffraction. In the earlier work by Dwight [8], Marazza [14], and Riani [16] the $CaIn_2$-type (space group $P6_3/mmc$) with a statistical distribution of copper and tin was assumed, while an ordered arrangement of copper and tin was reported by Yang *et al.* [10] and Adroja *et al.* [15]. The best powder data (neutron data) have recently been reported by Weill *et al.* [21]. They clearly established the ordering and a slight puckering of the $[Cu_3Sn_3]$ hexagons. Concerning the sample preparation, two different routes have been established: (i) arc-melting of the elements directly followed by annealing in sealed silica tubes between 750 and 850 °C for up to four weeks, or (ii) crystal growth *via* the Czochralski technique.

Magnetic, resistivity and specific heat studies on single crystal and polycrystalline CeCuSn have shown a complex magnetic ordering in this compound [11 – 12, 20]. Sakurai *et al.* observed antiferromagnetic ordering (T_N) around 8 K in arc-melted CeCuSn, which also exhibited weak spontaneous magnetization. However, the samples (which were eventually polycrystalline) prepared by the Czochralski pulling method

Table 1. Crystal data and structure refinement for CeCuSn, molar mass = 322.35 g mol^{-1}, $Z = 2$, $F(000) = 274$ e.

Preparation	— quenched —		annealed
Temperature [°C]	22	−150	22
Instrument	CAD4	Smart Apex I	IPDS II
Unit cell dimensions [pm]	$a = 458.2(1)$	$a = 455.8(2)$	$a = 458.4(1)$
(Guinier powder data) [pm]	$c = 793.7(2)$	$c = 791.6(6)$	$c = 785.8(2)$
[nm^3]	$V = 0.1443$	$V = 0.1424$	$V = 0.1430$
Space group	$P6_3/mmc$	$P6_3/mmc$	$P6_3mc$
Calculated density [g cm^{-3}]	7.42	7.52	7.49
Crystal size [μm^3]	— $25 \times 45 \times 65$ —		$20 \times 20 \times 70$
Transm. ratio (max/min)	1.40	1.36	1.77
Absorption coefficient [mm^{-1}]	31.0	31.4	31.3
θ range [°]	5 to 35	5 to 31	5 to 34
Range in *hkl*	±7, ±7, ±12	±6, −6/+3, −8/+11	±7, ±7, ±11
Total no. reflections	2334	963	1895
Independent reflections	148 ($R_{int} = 0.0569$)	102 ($R_{int} = 0.0526$)	233 ($R_{int} = 0.0301$)
Reflections with $I \geq 2\sigma(I)$	129 ($R_{sigma} = 0.0161$)	88 ($R_{sigma} = 0.0277$)	207 ($R_{sigma} = 0.0201$)
Data/parameters	148 / 8	102 / 8	233 / 11
Goodness-of-fit on F^2	1.200	1.166	1.106
Final R indices [$I \geq 2\sigma(I)$]	$R1 = 0.0332$	$R1 = 0.0376$	$R1 = 0.0282$
	$wR2 = 0.0705$	$wR2 = 0.0792$	$wR2 = 0.0752$
R indices (all data)	$R1 = 0.0397$	$R1 = 0.0499$	$R1 = 0.0354$
	$wR2 = 0.0727$	$wR2 = 0.0830$	$wR2 = 0.0764$
Extinction coefficient	0.012(2)	0.0002(18)	0.013(3)
BASF	–	–	0.55(10)
Largest diff. peak / hole [e Å^{-3}]	6.08 / −2.02	4.56 / −2.98	2.00 / −2.16

exhibited T_N around 10 K without any spontaneous magnetization [11]. Specific heat studies of Yang *et al.* showed two magnetic transitions around 8.6 and 7.3 K [10]. These anomalies in CeCuSn were further supported by the μSR studies by Kalvius *et al.*, who observed the presence of two magnetic states below 11 K [17]. A recent single crystal neutron diffraction experiment has demonstrated that the onset of antiferromagnetic ordering occurs around 12 K and an inflection around 8 K is seen in the temperature dependence of the magnetic intensities. The magnetic ground state is characterized by a magnetic wave vector k = $(0.115, 0, 0)$ [20]. CeCuSn has repeatedly been studied in order to understand the ground-state properties [19].

The complex magnetic behaviour of CeCuSn motivated us to investigate the magnetic structure of this interesting compound using ^{119}Sn Mössbauer spectroscopy. However during the synthesis, depending on the synthetic conditions, we observed two structural modifications of this compound.

The first method of synthesis was arc-melting the elements, and annealing a part of this *as cast* sample to obtain the second sample. Firstly β-CeCuSn was obtained by arc-melting the elements in ideal atomic ratio and quenching the ingot. This sample revealed a significantly larger c parameter and a magnetic ordering behaviour different from the one reported in the literature [10 – 12, 15 – 17, 20]. The second structural modification, α-CeCuSn, was obtained after annealing the first sample (*i. e.*, β-CeCuSn) in a sealed silica tube at 700 °C for one month. The lattice parameters for this sample were close to the values reported in the literature. We report herein a precise single crystal study on the high- (β) and low-temperature (α) modifications of CeCuSn. The relation between the structures and their physical properties was investigated by magnetic specific heat and ^{119}Sn Mössbauer spectroscopic studies on polycrystalline samples of both modifications.

Experimental Section

Syntheses

Starting materials for the preparation of the CeCuSn samples were a larger cerium ingot (Johnson Matthey), copper wire (Johnson Matthey, ∅ 1 mm), and tin granules (Heraeus), all with stated purities better than 99.9 %. In the first step, pieces of the cerium ingot were arc-melted [22] to small buttons under an argon atmosphere of *ca.* 800 mbar. The argon was purified before over titanium sponge (900 K), silica gel, and molecular sieves. The pre-melting procedure strongly reduces shattering during the subsequent reaction with copper and tin. The cerium buttons were then mixed with pieces of the copper wire and the tin granules in the ideal 1 : 1 : 1 atomic ratio and all were reacted together in the arc-melting furnace under argon (800 mbar). The product button was

melted three times to ensure homogeneity. The total weight losses after the arc-melting procedures were all smaller than 0.5 weight-percent. As defined above, we call this as cast CeCuSn the high-temperature modification, *i. e.*, β-CeCuSn. β-CeCuSn was obtained in an amount of 1 g. Part of the sample was subsequently sealed in an evacuated silica tube and annealed at 700 °C for four weeks to obtain the low-temperature modification, *i. e.*, α-CeCuSn. Compact pieces of polycrystalline α- and β-CeCuSn are stable in air over months while small single crystals and the finely grained grey powder deteriorate in humid air. Both CeCuSn samples were kept in Schlenk tubes prior to the investigations. Single crystals of CeCuSn exhibit metallic lustre.

X-Ray powder and single crystal diffraction

The arc-melted (β-CeCuSn) and annealed (α-CeCuSn) samples were checked through powder patterns taken in a Guinier camera (equipped with an image plate system Fujifilm, BAS-1800) using Cu$K_{\alpha 1}$ radiation and α-quartz (a = 491.30, c = 540.46 pm) as an internal standard. No impurities were found in both samples up to the level of X-ray detection. The hexagonal lattice parameters (Table 1) were obtained by least-squares refinements of the powder data. To ensure correct indexing, the observed patterns were compared to calculated ones [23] using the positional parameters obtained from the structure refinements. The lattice parameters of α-CeCuSn obtained in the present study are in good agreement with the data reported in literature [8 – 21]. The powder patterns of β-CeCuSn showed broader reflections (exhibiting lower crystallinity) as compared to those of α-CeCuSn. However, in addition, a small anisotropy concerning reflections with odd l indices was observed; *i.e. hk1* reflections were broader than *hk0* reflections in a close 2θ range.

Small, irregularly shaped single crystals were isolated from the quenched and from the annealed samples by mechanical fragmentation. The crystals were first examined with white Mo radiation on a Buerger precession camera (equipped with an image plate system, Fujifilm, BAS-1800) in order to establish suitability for intensity data collection. Intensity data of a crystal from the quenched arc-melted sample were collected at r. t. by use of a four-circle diffractometer (CAD4) with graphite monochromatized MoK_α radiation (71.073 pm) and a scintillation counter with pulse height discrimination. The scans were performed in the $\omega/2\theta$ mode. An empirical absorption correction was applied on the basis of Ψ scan data followed by a spherical absorption correction.

Additionally, low-temperature intensity data of the crystal selected from the quenched arc-melted sample were collected at −150 °C on a Bruker AXS Smart Apex I with a rotating anode (graphite-monochromatized MoK_α; 50 kV, 140 mA) and a fixed detector distance of 50 mm. Ω scans were employed with a step width of 0.3° at three consequent φ positions (0, 120, and 240°), thus allowing a semi-empirical absorption correction. The Ω range was 180°, *i. e.* $-90° \leq \theta \leq 90°$. A 30 s counting time was used for each frame. The data acquisition and the absorption correction were carried out with SAINT PLUS 6.28A and SADABS, respectively, supplied by Bruker-AXS. Intensity data of the annealed CeCuSn crystal were collected on a Stoe IPDS-II image plate diffractometer using monochromatized MoK_α radiation (71.073 pm). A numerical absorption correction was applied to the data. All relevant crystallographic data and details for the three data collections and evaluations are listed in Table 1.

Physical property measurements and ^{119}Sn Mössbauer spectroscopy

Samples in bulk form were used for the magnetic and specific heat measurements. The magnetic measurements were carried out on QD-PPMS instrument using the VSM insert. The heat capacity (C_p) measurements were also performed on the same PPMS (HC option) using *Apiezon N* grease as glue for sticking the sample onto the platform of the puck.

A $Ca^{119m}SnO_3$ source was available for the ^{119}Sn Mössbauer spectroscopic investigations. The samples were placed within a thin-walled PVC container at a thickness of about 10 mg Sn cm^{-2}. A palladium foil of 0.05 mm thickness was used to reduce the Sn-K X-rays concurrently emitted by this source. The measurements were conducted in the usual transmission geometry at 78 and 4.2 K.

Results and Discussion

Structure refinements

The data collections clearly revealed doubling of the pronounced AlB_2 related subcells, as was already evident from the Guinier powder data. Analysis of the systematic extinctions revealed the 6_3 screw axis for the three data sets, leading to the possible space groups $P6_3mc$ (NdPtSb-type) or $P6_3/mmc$ (ZrBeSi-type). The structure of the crystal from the arc-melted and quenched sample was refined first. In view of the recently refined LaCuSn structure [1], the ZrBeSi model, space group $P6_3/mmc$ was tested first. The LaCuSn atomic positions were taken as starting values and the structure was refined using SHELXL-97 (full-matrix least-squares on F^2) [24] with anisotropic atomic displacement parameters for all atoms. While the cerium atoms show an almost isotropic displacement, especially the copper atoms behave anisotropically with an extreme displacement in the c direction (high U_{33} parameter). This was a clear hint to a violation of the mirror planes at z = 1/4 and z =

Atom	Wyckoff position	x	y	z	U_{11}	U_{33}	U_{12}	U_{eq}
Quenched, 22 °C, $P6_3/mmc$								
Ce	2*a*	0	0	0	127(4)	93(5)	64(2)	116(3)
Cu	2*c*	1/3	2/3	1/4	108(8)	789(32)	54(4)	335(10)
Sn	2*d*	1/3	2/3	3/4	69(4)	172(6)	35(2)	103(4)
Quenched, −150 °C, $P6_3/mmc$								
Ce	2*a*	0	0	0	83(6)	90(8)	42(3)	86(6)
Cu	2*c*	1/3	2/3	1/4	51(12)	1145(56)	26(6)	416(18)
Sn	2*d*	1/3	2/3	3/4	26(7)	170(10)	13(3)	74(6)
Quenched, annealed at 700 °C, 22 °C, $P6_3/mc$								
Ce	2*a*	0	0	0[a]	113(3)	95(5)	57(1)	107(3)
Cu	2*b*	1/3	2/3	0.2733(7)	105(5)	401(45)	53(3)	204(15)
Sn	2*b*	1/3	2/3	0.7343(5)	72(3)	192(10)	36(1)	112(4)

Table 2. Atomic coordinates and anisotropic displacement parameters (pm^2) for CeCuSn. U_{eq} is defined as one third of the trace of the orthogonalized U_{ij} tensor. $U_{11} = U_{22}$, $U_{13} = U_{23} = 0$.

[a] The cerium atom was kept fixed at the origin of the cell.

Quenched, 22 °C				Quenched, −150 °C				Quenched, annealed, 22 °C			
Ce:	6	Sn	330.7	Ce:	6	Sn	329.3	Ce:	3	Cu	319.0
	6	Cu	330.7		6	Cu	329.3		3	Sn	322.4
									3	Sn	337.1
									3	Cu	340.8
Cu:	3	Sn	264.5	Cu:	3	Sn	263.2	Cu:	3	Sn	266.4
	6	Ce	330.7		6	Ce	329.3		3	Ce	319.0
									3	Ce	340.8
Sn:	3	Cu	264.5	Sn:	3	Cu	263.2	Sn:	3	Cu	266.4
	6	Ce	330.7		6	Ce	329.3		3	Ce	322.4
									3	Ce	337.1

Table 3. Interatomic distances (pm) calculated with the lattice parameters taken from X-ray powder data of CeCuSn. All distances within the first coordination spheres are listed. Standard deviations are equal or less than 0.1 pm.

3/4, thus indicating a puckering of the Cu_3Sn_3 network. In the next step the structure was refined in the non-centrosymmetric space group $P6_3mc$ with puckered $[Cu_3Sn_3]$ layers. This along with twinning by inversion did not solve the strong anisotropic displacement of the copper atoms. Both the copper and the tin atoms remained on the ideal positions at $z = 1/4$ and $z = 3/4$ within two standard uncertainties, and the large U_{33} values were as high as in the centrosymmetric refinement. This has clearly manifested that in the high-temperature phase microdomains are present which have ordered, slightly puckered Cu_3Sn_3 hexagons within a single domain, but are out of phase among one another. *Anti* phase boundaries (APB) are possible in view of the symmetry reduction (*klassengleiche* transition, k2) in going from the AlB_2 subcell to the superstructure with ZrBeSi-type [2]. Due to the small domain size, *i. e.* the high density of APBs along *c*, the average structure is described best as ZrBeSi-type even though the layers are slightly puckered locally. For the final runs the $P6_3/mmc$ model was assumed again for this crystal.

The same crystal from the arc-melted and quenched sample was then investigated at −150 °C in order to check whether a temperature-induced dynamic behaviour can be ruled out. The refinement in space group $P6_3/mmc$ revealed almost the same results, however, with a slightly higher anisotropy for the copper and tin atoms, indicating a stronger tendency for puckering. A refinement with split positions (1/3, 2/3, *z* instead of 1/3, 2/3, 1/4) for the copper atoms did not improve the residuals and has further manifested the disorder (short range order) in the quenched sample. We have therefore described this crystal also in space group $P6_3/mmc$.

Finally the structure of the annealed sample was refined. From the Guinier powder pattern it was already evident that the *c* lattice parameter of the annealed sample was significantly smaller (793.7 *vs.* 785.8 pm). This was a clear indication for a puckering and ordering of the $[Cu_3Sn_3]$ networks. Consequently we have refined the α-CeCuSn structure in space group $P6_3mc$, and the atomic parameters of YCuSn [1] were taken as starting values. The structure refinement went smoothly to the residuals listed in Table 1 and the pronounced anisotropy disappeared. The occupancy parameters were refined in a separate series of least-squares cycles. All sites were fully occupied within two standard uncertainties. A final difference electron-density synthesis was flat and did not reveal any significant residual peaks. The results of the three structure refinements are summarized in Table 1. The atomic co-

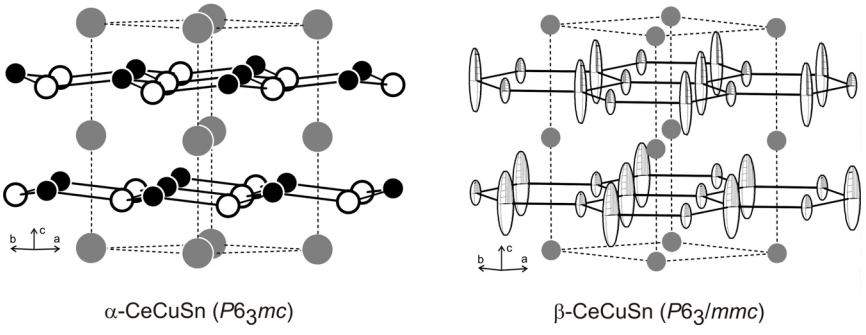

Fig. 1. The crystal structures of α- and β-CeCuSn. The cerium, copper, tin atoms are drawn as medium grey, filled, and open circles, respectively. The displacement ellipsoids for β-CeCuSn are drawn at the 99 % probability level. The two-dimensional [CuSn] networks are emphasized. For details see text.

ordinates and the interatomic distances are listed in Tables 2 and 3. Further information on the structure refinements is available [25].

Crystal chemistry

X-Ray powder diffraction data revealed significant differences for the *c* lattice parameters, *i. e.* 793.7(2) pm for the quenched (β-CeCuSn) and 785.8(2) pm for the annealed (α-CeCuSn) sample, along with larger FWHM (full width at half maximum) for odd *l* indices. To the best of our knowledge, the short range order high-temperature modification is described here for the first time. In all investigations given in the literature [8 – 21] either annealed samples or Czochralski grown single crystals were used. Most *c* lattice parameters listed in references [8 – 21] are close to 786 pm, comparable with α-CeCuSn. In some older literature [8, 9, 14, 16], the $CaIn_2$-type with a statistical Cu/Sn occupancy had been assigned to CeCuSn, which is definitely wrong, since in β-CeCuSn ordered $[Cu_3Sn_3]$ hexagons already occur (Fig. 1).

Similar to the recently reported data on LaCuSn [1], CeCuSn shows short range order when quenching the sample from the melt. Due to the large size of the cerium atoms, the [CuSn] networks are well separated from each other, and there are no interlayer interactions. After the quenching process the $[Cu_3Sn_3]$ hexagons are already ordered, but there is no long-range ordering with respect to the puckering along *c*. We find statistical dislocations above and below the subcell mirror planes, leading to the strong anisotropic displacements. The disorder of the [CuSn] layers among one another requires space. Consequently we observe a higher *c* lattice parameter and thus higher cell volume for the high-temperature phase (0.1430 *vs*. 0.1443 nm^3). Therefore APBs are assumed to occur along *c*.

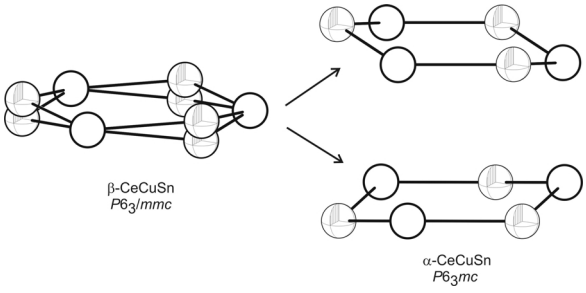

Fig. 2. Cutouts of the α- and β-CeCuSn structures. Only one Cu_3Sn_3 hexagon is emphasized. The copper and tin positions are drawn as octants and open circles, respectively. In β-CeCuSn only a superposition of the ordered arrangements of α-CeCuSn is seen by X-ray diffraction. The local picture of α-CeCuSn is valid also for β-CeCuSn, except for a lesser puckering and the occurrence of microdomains. For details see text.

In Fig. 2 we illustrate the effect of the apparent disorder suggested by the X-ray diffraction results. In the high-temperature modification we detect a superposition of both conformational forms present in the low-temperature phase. These are statistically frozen in when quenching the sample from the melt. The microdomains could not be resolved by X-ray diffraction and as a consequence we observe the large anisotropic displacement of the copper atoms. In various literature reports on CeCuSn [8 – 21] the *c* lattice parameter varies from 784.85 [21] to 793.7 pm (this work for β-CeCuSn). Based on the present results we assume that all samples with the higher *c* values have some disorder between the adjacent [CuSn] layers; *i. e.* varying densities of APBs.

In contrast, the annealed sample clearly shows the ordered NdPtSb-type structure, similar to the *R*CuSn stannides with the heavier rare earth elements [1, and ref. therein]. The space group symmetry is reduced from $P6_3/mmc$ (ZrBeSi-type) to $P6_3mc$ (NdPtSb-type) *via* a *translationengleiche* symmetry reduction of in-

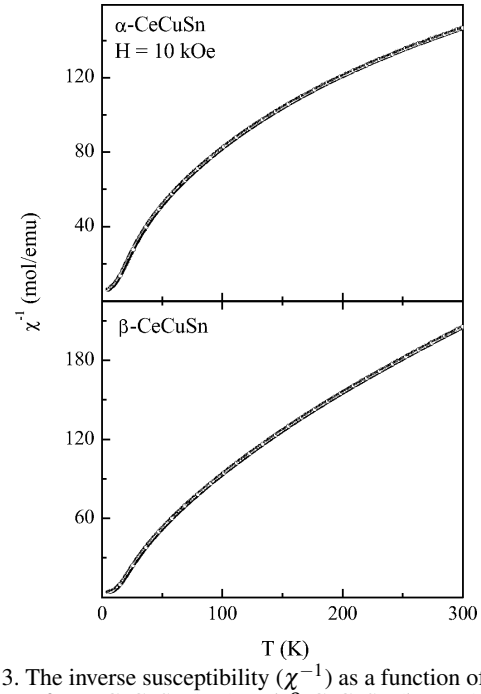

Fig. 3. The inverse susceptibility (χ^{-1}) as a function of temperature for α-CeCuSn (top) and β-CeCuSn (bottom) measured in a field of 10 kOe. The above data was fitted to a modified Curie-Weiss law including a temperature independent term, χ_0. For details see text.

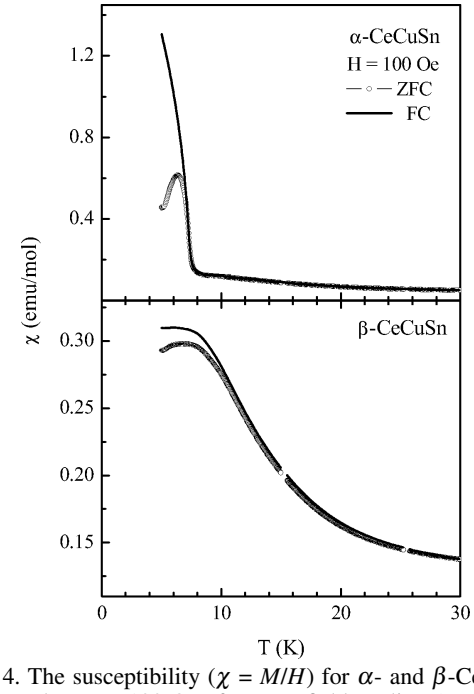

Fig. 4. The susceptibility ($\chi = M/H$) for α- and β-CeCuSn measured at H = 100 Oe after zero field cooling (ZFC) and field cooling (FC) the sample.

dex 2 (t2) with a loss of the centre of symmetry [2]. Consequently we observed twinning by inversion for the investigated crystal where the twin domains are large enough for independent coherent scattering. For the α-CeCuSn structure we only observe a small anisotropy of the copper displacements, similar to ScCuSn, YCuSn, and LuCuSn [1], and there are no significant residual peaks in the final difference Fourier synthesis. Our single crystal data are in excellent agreement with a recent neutron powder diffraction study [21], but with better precision for the positional parameters. For a more detailed discussion of the chemical bonding and the dimensionality of the [CuSn] networks within the series of *RE*CuSn stannides we refer to previous work [1, 2].

Physical property measurements

In Fig. 3 we show the susceptibility ($\chi = M/H$) plotted as χ^{-1} *vs.* T for both modifications of CeCuSn, measured in an applied field of 10 kOe. The curvature in the plots of χ^{-1} *vs.* T has also been observed in previous studies [10 – 11, 13]. The susceptibility above 100 K could be fitted to a Curie-Weiss law modified by adding a temperature-independent term and given as $\chi = \chi_0 + C/(T - \theta_p)$, where χ_0 is the temperature-independent Pauli contribution, C is the Curie constant and θ_p is the paramagnetic Curie temperature. The effective Bohr magnetons number (μ_{eff}) can thus be calculated from the Curie constant [26]. The values of χ_0, θ_p and μ_{eff} for α-CeCuSn are 4.15×10^{-3} emu mol^{-1}, 10 K and 2.49 μ_B per Ce atom, respectively. Similarly for β-CeCuSn these values are 2.2×10^{-3} emu mol^{-1}, 19 K and 2.46 μ_B per Ce atom. The values of μ_{eff} for both compounds are in close agreement with the value of the effective Bohr magnetons number for free Ce^{3+}, 2.54 μ_B, indicating trivalent cerium in the α- and β-modification of CeCuSn. The positive values of θ_p indicate ferromagnetic interactions.

A very clear difference in the magnetism of these two modifications can be seen from the low field susceptibility curves plotted in Fig. 4. The top panel shows the zero field cooled (ZFC) and field cooled (FC) $\chi(T)$ curves for α-CeCuSn measured in a field of 100 Oe. Earlier heat capacity studies of annealed CeCuSn have shown two magnetic transitions at 8.6 and 7.4 K [12]. Consistent with these temperatures, there is a sudden rise in $\chi(T)$ of α-CeCuSn around 8.6 K as if it were a ferromagnetic ordering (*vide infra*). The observa-

tion of a ferromagnetic component is consistent with the observations made by Sakurai *et al.* for CeCuSn (high value of residual resistivity, mixing of a small ferromagnetic component). The positive value of θ_p however contradicts the observation of a negative θ_p by Yang *et al.* [10, 11]. The ZFC-FC line bifurcates around 7.2 K, and the ZFC undergoes an antiferromagnetic transition with a broad peak around 6.3 K. In the bottom panel of Fig. 4, the ZFC-FC curves for β-CeCuSn are shown. The features are totally different from the one seen for α-CeCuSn. The susceptibility in ZFC and FC state increases with decreasing temperature and exhibits a broad peak below 10 K, which can be attributed as short-range magnetic ordering [27]. This feature is directly correlated to the missing long-range structural ordering of the Cu_3Sn_3 hexagons in β-CeCuSn (see Fig. 2).

The difference in the magnetism of α-CeCuSn and β-CeCuSn can also be seen in the behaviour of the $M(H)$ curves. In Fig. 5 we have shown the magnetization as a function of field up to 80 kOe at 5 K. It is interesting to observe the occurrence of small steps in the magnetization of α-CeCuSn at fields of 8, 10, 20 and 30 kOe both in up (field ramping up) and down (field ramping down) cycles, indicating spin reorientation effects. A small remanent magnetization is seen at low fields, and can be more clearly seen in the hysteresis loop (discussed below). $M(H)$ at 5 K for β-CeCuSn is shown in the bottom panel of Fig. 5. M increases with H without any steps in the magnetization as was observed in the case of α-CeCuSn. The $M(H)$ curve clearly resembles features of an antiferromagnet, *i. e.*, non-linear increase in M with increasing H with a tendency to saturate at higher fields. The saturation moment value at 80 kOe, for both compounds is about 1 μ_B per mole which is usually observed for ternary trivalent cerium compounds with localized *4f* magnetism [28]. The reduced moment values, referring to the expected $g_J\, J = 2.14\ \mu_B\ \mathrm{mol}^{-1}$ for Ce^{3+}, can be attributed to the crystal field splitting effects on the $J = 5/2$ ground state of the Ce^{3+} ion. Compounds exhibiting saturation moment values (in units of μ_B) similar to CeCuSn are the following: 1.09 – CeAuGe [29], 1.2 – CePdSb [30], or 1.12 – CeAgGa [31].

A hysteresis loop measured at 5 K for α-CeCuSn up to $\pm$10 kOe is shown as the inset in the top panel of Fig. 5. A small remanent field, few Oersteds wide can be clearly seen. The loop collapses when the field crosses this critical value. Such a hysteresis loop is usually seen for compounds exhibiting cluster-glass like behaviour [32]. This means that a small amount of a ferromagnetic component is present in this compound. Therefore it can be assumed that in α-CeCuSn there exists, along with antiferromagnetic ordering, a spontaneous magnetization at low temperatures resulting in the formation of cluster-glass like anomalies. This phenomenon for α-CeCuSn is not clearly understood at present and needs further detailed experimental investigations. As shown in the inset of the bottom panel of Fig. 5, for β-CeCuSn there is no hysteresis at 5 K, and the curve is almost linear with almost no broadening around the origin. In the context of different magnetic behaviour it is very interesting to see that introducing long range order of the puckering in the [CuSn] network significantly alters the magnetism of CeCuSn.

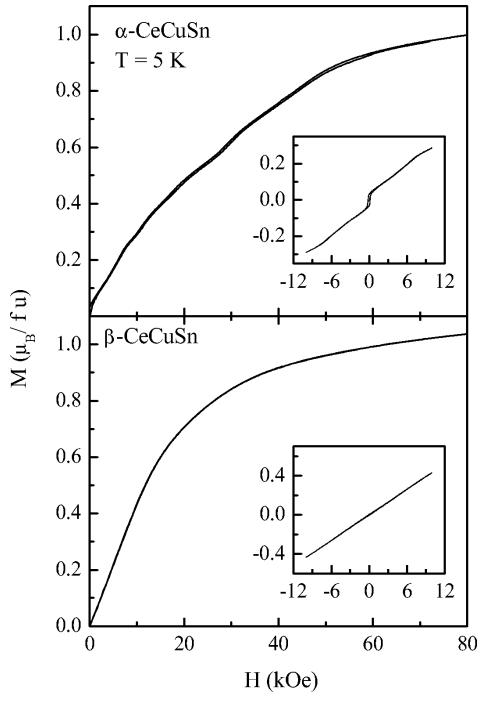

Fig. 5. Magnetization as a function of varying field for α- and β-CeCuSn measured at 5 K. The inset in both panels shows the hysteresis loop recorded at the same temperature for the respective compound.

Now we focus on the specific heat behaviour of the α- and β- forms of CeCuSn in Fig. 6. The peaks in $C(T)$ of α-CeCuSn are observed at 8.6(1) and 7.5(1) K which is consistent with the observation of two transitions in the C_p data of the annealed CeCuSn samples [10, 12]. We consider 8.6 K as T_N in accordance with results of previous C_p studies on CeCuSn [12].

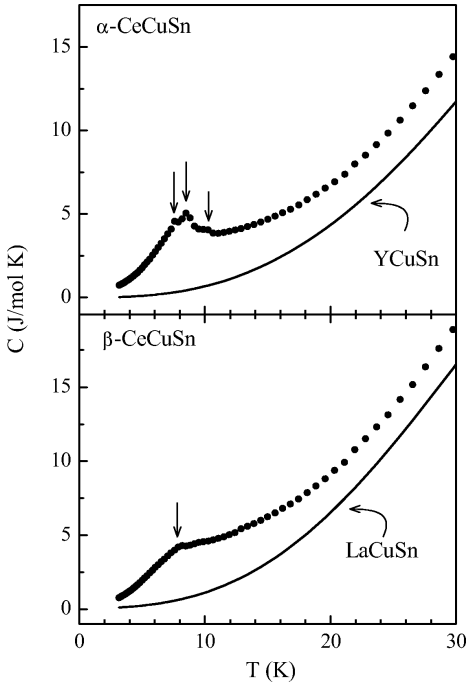

Fig. 6. Total heat capacity (C) for α- and β-CeCuSn. In both panels plotted is the heat capacity of their respective non-magnetic counterparts, YCuSn and LaCuSn.

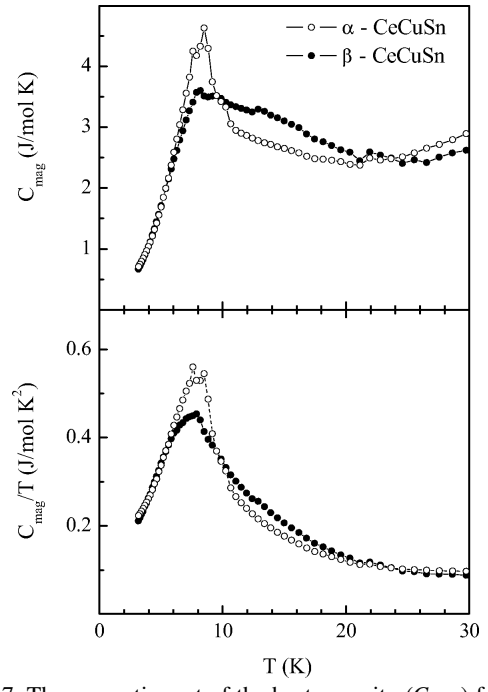

Fig. 7. The magnetic part of the heat capacity ($C_{\rm mag}$) for α- and β-CeCuSn plotted in different ways. $C_{\rm mag}$ is obtained by subtracting the lattice part (*i. e.* the heat capacity of non-magnetic YCuSn and LaCuSn) from the total heat capacity of α- and β-CeCuSn. See text for details.

There is a small anomaly around 10 K, consistent with the earlier reports that the onset of antiferromagnetic ordering takes place around this temperature. The $C(T)$ for β-CeCuSn is shown in the bottom panel of Fig. 6. Contrary to α-CeCuSn, there is only one step-like anomaly around 7.9(1) K which we consider as $T_{\rm N}$ for β-CeCuSn. It may be recalled that the magnetic phase diagram of CeCuSn given by Nakotte *et al*. indicates that magnetic anisotropy is intrinsic to the CeCuSn compound [12].

In order to understand the ground state of CeCuSn, it is important to get the magnetic part of the heat capacity for both modifications. Structurally, YCuSn [1] is similar to α-CeCuSn, and LaCuSn [1] is close to β-CeCuSn; therefore we have taken these compounds as non-magnetic references for subtracting the lattice part in order to obtain the magnetic part of heat capacity for α- and β-CeCuSn. The $C(T)$ curves for YCuSn and LaCuSn are also shown in the top and bottom panels, respectively. The magnetic part of the heat capacity for α- and β-CeCuSn is shown in different forms in Fig. 7. A λ anomaly corresponding to the magnetic transitions is clearly seen in both modifications of CeCuSn. The difference in magnetic behaviour of the two modifications of CeCuSn is evident. In α-CeCuSn the two peaks corresponding to the ordering temperatures are clearly seen in $C_{\rm mag}$ with a sudden rise around 12 K. For β-CeCuSn small peaks around 8 and 13 K are seen in $C_{\rm mag}$. In both compounds a small bump in $C_{\rm mag}$ is seen at 24(1) K. A careful look at Fig. 5 of Ref. [10] shows that the curves of $C_{\rm p}/T$ *vs.* T measured in different applied fields cross each other around 25 K, indicating heavy fermion like behaviour in CeCuSn [10, 33].

The plot of $C_{\rm mag}/T$ *vs.* T^2 for the entire temperature range of measurement is shown in the main panel of Fig. 8. To highlight the low temperature part, *i. e.*, to clearly see the T^3 behaviour of $C_{\rm mag}$, we have plotted $C_{\rm mag}/T$ *vs.* T^2 on an expanded scale as an inset. In the ordered region, below 5 K, $C_{\rm mag}$ follows T^3 and from the fit of this linear region we obtain the electronic coefficient of heat capacity (γ) to be 140 and 132 mJ mol^{-1} K^2 for α- and β-CeCuSn, respectively. The value of $\gamma > 100$ mJ mol^{-1} K^2 puts both forms of CeCuSn in the class of moderate heavy fermion materials.

Table 4. Fitting parameters of ^{119}Sn Mössbauer measurements of α- and β-CeCuSn at 78 and 4.2 K. Numbers in parentheses represent the statistical errors in the last digit. (δ), isomeric shift; ΔE_Q, electric quadrupole splitting; $|B_{hf}|$, magnetic hyperfine field; (Γ), experimental line width.

Compound	Temperature (K)	δ (mm s^{-1})	ΔE_Q (mm s^{-1})	B_{hf} (T)	Γ (mm s^{-1})
α-CeCuSn	78	1.94(1)	0.45(3)	–	1.12(3)
	4.2	1.99(3)	0.05(2)	1.03(1)	1.98(1)
β-CeCuSn	78	1.89(2)	0.32(8)	–	1.02(7)
	4.2	1.93(1)	0.12(2)	1.97(4)	1.83(3)

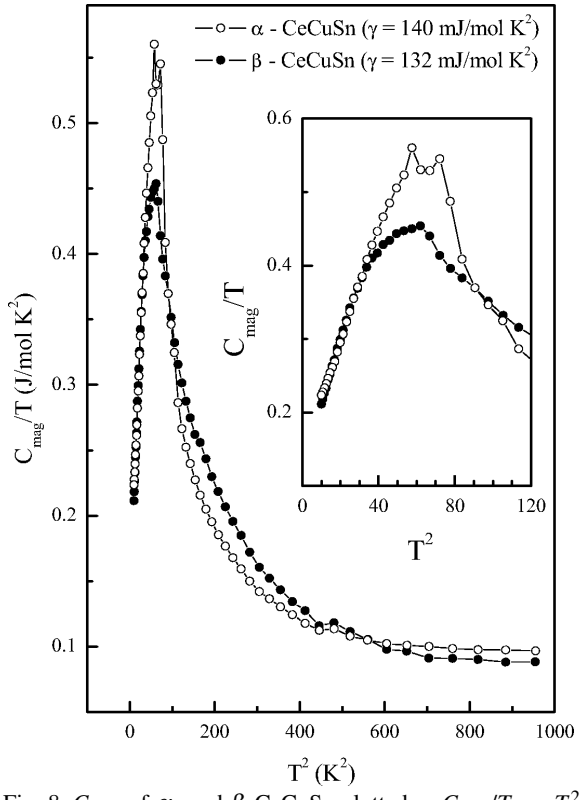

Fig. 8. C_{mag} of α- and β-CeCuSn plotted as C_{mag}/T *vs.* T^2 in the full scale of measurement, to show the anomalies observed at different temperatures. C_{mag}/T *vs.* T^2 is shown in an expanded form in the inset to highlight the T^3 behaviour of C_{mag} in the ordered region.

^{119}Sn Mössbauer spectroscopy

^{119}Sn Mössbauer spectra of the α- and β-CeCuSn samples measured at 78 and 4.2 K are shown in Figs. 9 and 10, respectively. In agreement with the crystal structures, the spectra are easily understood in terms of single crystallographic tin sites. The hyperfine parameters derived at the above mentioned temperatures from the recorded spectra are presented in Table 4. As expected, above T_N, the non-cubic tin site symmetry (3*m*.) in α-CeCuSn results in a small quadrupolar splitting 0.45(3) mm s^{-1} which agrees well with the values measured for the Sn site in the isostructural compounds *R*CuSn (*R* = Gd–Er) [34]. In contrast, the quadrupole splitting value of 0.32(8) mm s^{-1} measured for β-CeCuSn is significantly smaller, consistent with the higher Sn site symmetry ($\bar{6}m2$) in this compound which is close to the value of LaCuSn [1]. The smaller quadrupole splitting for α-CeCuSn indicates a decrease in the electric field gradient at the tin site in α-CeCuSn as compared to β-CeCuSn. The isomer shifts are in the typical range observed for tin in intermetallic compounds [35 – 39] and comparable to those measured for the corresponding gold and silver stannides.

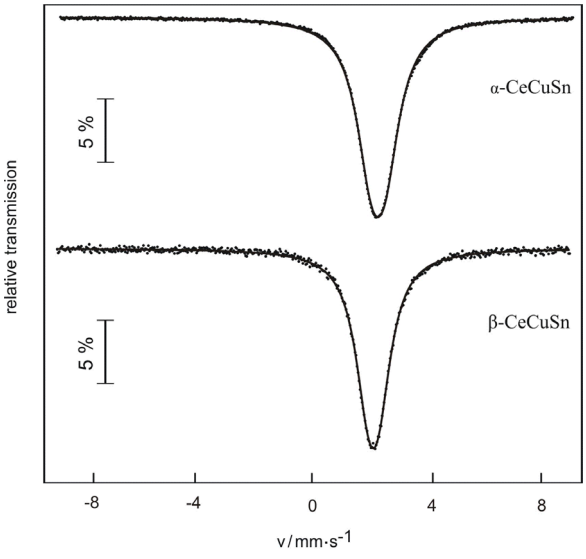

Fig. 9. Experimental (data points) and simulated (continuous line) ^{119}Sn Mössbauer spectra of α- and β-CeCuSn at 78 K.

The Mössbauer spectra at 4.2 K (Fig. 10) show magnetic hyperfine field splitting below T_N for α- and β-CeCuSn. The transferred hyperfine fields are 1.03(1) and 1.97(4) *T* for α- and β-CeCuSn, respectively.

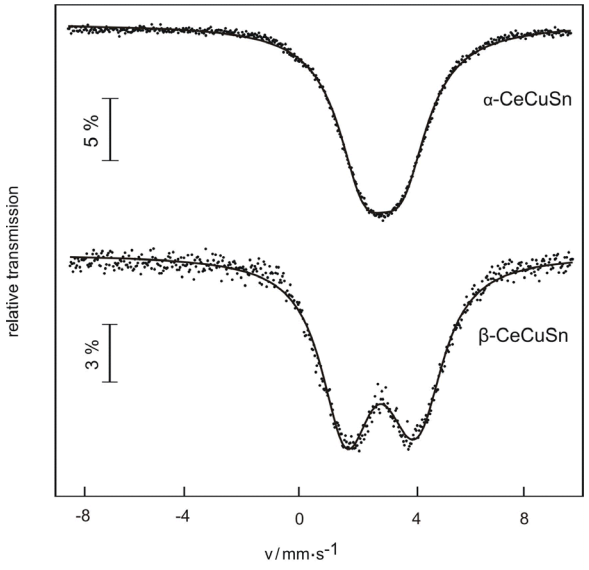

Fig. 10. Experimental (data points) and simulated (continuous line) ^{119}Sn Mössbauer spectra of α- and β-CeCuSn at 4.2 K.

Since the values for the transferred hyperfine fields are small, and thus correlated with the line width parameter, the absolute values should not be overinterpreted. They suggest a structurally frustrated cerium in β-CeCuSn.

Summary

We were able to obtain two structural modifications of CeCuSn by varying the synthesis conditions (the β modification being obtained by quenching the arc-melted sample and the α modification by annealing the quenched sample). The successful analysis of single crystal data gives precise information about the structure of CeCuSn, which helps in interpreting the anomalies observed in the physical properties. By quenching the sample, a short range order of locally slightly puckered [CuSn] layers is obtained. Anti phase boundaries (APB) disturb the order of the layers in the *c* direction. Annealing reduces the effect of APBs completely, the puckering becomes stronger and a three-dimensional long range order is present which strongly affects the magnetism of this compound. The magnetic and specific heat studies on α-CeCuSn have revealed a complex magnetic ordering. This compound exhibits closely spaced steps in the magnetization measurement at 5 K and signatures of a spin glass with small remanent field around the origin in the hysteresis loop. On the other hand, β-CeCuSn behaves as an antiferromagnet with no steps in the $M(H)$ curve. The differences in magnetic behaviour of α- and β-CeCuSn are therefore believed to be the manifestation of their structural differences. We believe that the results presented here will stimulate further work to completely understand the 'complex' magnetic behaviour of CeCuSn.

Acknowledgements

This work was financially supported by the Deutsche Forschungsgemeinschaft. C.P.S. and S.R. are indebted to the NRW Graduate School of Chemistry and to the Alexander von Humboldt-Foundation, respectively, for research grants.

[1] C. P. Sebastian, H. Eckert, R.-D. Hoffmann, R. Pöttgen, *Solid State Sci*., in press.
[2] R.-D. Hoffmann, R. Pöttgen, *Z. Kristallogr*. **2001**, *216*, 127.
[3] J. W. Nielsen, N. C. Baenziger, *Acta Crystallogr*. **1954**, *7*, 132.
[4] G. Wenski, A. Mewis, *Z. Kristallogr*. **1986**, *176*, 125.
[5] W. Bockelmann, H. Jacobs, H.-U. Schuster, *Z. Naturforsch*. **1970**, *25b*, 1305.
[6] W. Bockelmann, H.-U. Schuster, *Z. Anorg. Allg. Chem*. **1974**, *410*, 233.
[7] J. P. Maehlen, M. Stange, V. A. Yartys, R. G. Delaplane, *J. Alloys Compd*. **2005**, *404 – 406*, 112.
[8] A. E. Dwight, *Proc. Rare Earth Res. Conf*. **1976**, *1*, 480.
[9] L. P. Komarovskaya, R. V. Skolozdra, I. V. Filatova, *Dopov. Akad. Nauk. Ukr. RSR, Ser. A*, **1983**, 81.
[10] F. Yang, J. P. Kuang, J. Li, E. Brück, H. Nakotte, F. R. de Boer, X. Wu, Z. Li, Y. Wang, *J. Appl. Phys*. **1991**, *69*, 4705.
[11] J. Sakurai, K. Kegai, K. Nishimura, Y. Ishikawa, K. Mori, *Physica B* **1993**, *186 – 188*, 583.
[12] H. Nakotte, E. Brück, K. Prokes, J. H. V. J. Brabers, F. R. de Boer, L. Havela, K. H. J. Buschow, Y. Fu-ming, *J. Alloys Compd*. **1994**, *207/208*, 245.
[13] A. Ślebarski, A. Jezierski, A. Zygmunt, S. Mähl, M. Neumann, G. Borstel, *Phys. Rev. B* **1996**, *54*, 13551.
[14] R. Marazza, P. Riani, D. Mazzone, G. Zanicchi, R. Ferro, *Intermetallics* **1996**, *4*, 131.
[15] D. T. Adroja, B. D. Rainford, A. J. Neville, *J. Phys.: Condens. Matter* **1997**, *9*, L391.
[16] P. Riani, D. Mazzone, G. Zanicchi, R. Marazza, R. Ferro, *Intermetallics* **1997**, *5*, 507.
[17] G. M. Kalvius, A. Kratzer, H. Nakotte, D. R. Noakes,

C. E. Stronach, R. Wäppling, *Physica B* **2000**, *289–290*, 252.
[18] G. M. Kalvius, A. Kratzer, G. Grosse, D. R. Noakes, R. Wäppling, H. v. Löhneysen, T. Takabatake, Y. Echizen, *Physica B* **2000**, *289–290*, 256.
[19] D. R. Noakes, G. M. Kalvius, H. Nakotte, E. Schreier, R. Wäppling, *Physica B* **2002**, *312–313*, 292.
[20] S. Chang, Yu. Janssen, V. O. Garlea, J. Zarestky, H. Nakotte, R. J. McQueeney, *J. Appl. Phys*. **2005**, *97*, 10A913.
[21] F. Weill, M. Pasturel, J.-L. Bobet, B. Chevalier, *J. Phys. Chem. Solids* **2006**, *67*, 1111.
[22] R. Pöttgen, Th. Gulden, A. Simon, *GIT Labor-Fachzeitschrift* **1999**, *43*, 133.
[23] K. Yvon, W. Jeitschko, E. Parthé, *J. Appl. Crystallogr.* **1977**, *10*, 73.
[24] G. M. Sheldrick, SHELXL-97, Program for Crystal Structure Refinement, University of Göttingen, Göttingen (Germany) **1997**.
[25] Further details of the crystal structure investigations may be obtained from Fachinformationszentrum Karlsruhe, 76344 Eggenstein-Leopoldshafen, Germany (e-mail: crysdata@fiz-karlsruhe.de, http://www.fiz-informationsdienste.de/en/DB/icsd/depot_anforderung.html) on quoting the deposition numbers CSD-416788 (α-CeCuSn), CSD-416786 (β-CeCuSn, r. t. data set), and CSD-416787 (β-CeCuSn, -150 °C data set).
[26] C. Kittel, *Introduction to Solid State Physics*, 5th Edition, Wiley Eastern Limited, New Delhi, **1984**.
[27] L. J. De Jongh, A. R. Miedema, *Adv. Phys*. **1973**, *23*, 1.
[28] J. Jensen and A. R. Mackintosh, *Rare Earth Magnetism – Structures and Excitations*, Clarendon Press, Oxford, **1991**.
[29] R. Pöttgen, H. Borrmann, R. K. Kremer, *J. Magn. Magn. Mater*. **1996**, *152*, 196.
[30] S. K. Malik, D. T. Adroja, *Phys. Rev. B* **1991**, *43*, 6295.
[31] D. T. Adroja, B. D. Rainford, S. K. Malik, *Physica B* **1993**, *186–188*, 566.
[32] J. A. Mydosh, *Spin glasses – An experimental Introduction*, Taylor and Francis, London, **1993**.
[33] D. Vollhardt, *Phys. Rev. Lett*. **1997**, *78*, 1307.
[34] C. P. Sebastian, S. Rayaprol, R. Pöttgen, *Solid State Commun*. **2006**, *140*, 276.
[35] R. Pöttgen, P. E. Arpe, C. Felser, D. Kußmann, R. Müllmann, B. D. Mosel, B. Künnen, G. Kotzyba, *J. Solid State Chem*. **1999**, *145*, 668.
[36] D. Niepmann, R. Pöttgen, B. Künnen, G. Kotzyba, B. D. Mosel, *Chem. Mater*. **2000**, *12*, 533.
[37] D. Niepmann, R. Pöttgen, K. M. Poduska, F. J. Di Salvo, H. Trill, B. D. Mosel, *Z. Naturforsch*. **2001**, *56b*, 1.
[38] R. Müllmann, U. Ernet, B. D. Mosel, H. Eckert, R. K. Kremer, R.-D. Hoffmann, R. Pöttgen, *J. Mater. Chem*. **2001**, *11*, 1133.
[39] K. Łątka, J. Gurgul, R. Kmieć, A. W. Pacyna, W. Chajec, *J. Alloys Compd*. **2005**, *400*, 16.